



Engineering Notes

Computational Fluid Dynamics Analysis of an Optimized Load-Distribution Propeller

Jurij Sodja*

University of Ljubljana, 1000 Ljubljana, Slovenia

Domen Stadler†

Turboinstitut, 1210 Ljubljana, Slovenia

and

Tadej Kosel‡

University of Ljubljana, 1000 Ljubljana, Slovenia

DOI: 10.2514/1.C031469

Nomenclature

B	= number of propeller blades
C_D	= drag coefficient
C_L	= lift coefficient
C_P	= power coefficient, $P/\rho n^3 D^5$
C_T	= thrust coefficient, $T/\rho n^2 D^4$
c	= chord
D	= propeller diameter
G	= normalized circulation function
G_G	= Goldstein's normalized circulation function
G_P	= Prandtl's normalized circulation function
J	= advance ratio, v_0/nD
M	= Mach number
n	= propeller revolutions per second, $\Omega/2\pi$
P	= power
Q	= torque
R	= propeller radius
Re	= Reynolds number
R_H	= propeller hub radius
R_1	= wake radius
r	= radial coordinate
S	= propeller disk area, πR^2
T	= thrust
u_a	= axial induced velocity
u_ϕ	= angular induced velocity
v	= resultant velocity
v_0	= advance velocity
w	= axial vortex displacement velocity
y^+	= nondimensional wall distance
α	= angle of attack
β	= blade pitch angle
Γ	= circulation
ϵ	= drag-to-lift ratio

η	= propeller efficiency
Λ	= propeller blade pitch, $v_0 t_0 = 2\pi v_0 / \Omega$
Λ_1	= wake pitch
λ	= speed ratio, $v_0 / \Omega R$
λ_1	= wake speed ratio, $(v_0 + w) / \Omega R_1$
ξ	= nondimensional radius, r/R
ξ_1	= nondimensional wake radius, r/R_1
ρ	= fluid density
ϕ	= flow angle
Ω	= propeller angular velocity

I. Introduction

IT HAS been demonstrated by Larrabee [1], Adkins and Liebeck [2], and Gur and Rosen [3], among others, that a blade-element momentum (BEM) model performs well at predicting the thrust produced and the power required by the propeller. Computational fluid dynamics (CFD) analyses that take propeller integral properties into account were presented by Westmoreland et al. [4] and Sezer-Uzol and Long [5], suggesting that significant agreement between CFD and experimental results should be forthcoming. Furthermore, Roosenboom et al. [6] compared CFD results for velocity and vorticity fields in the propeller wake, where the data were obtained via the phase-locked particle image velocimetry method. Overall, adequate agreement was reported [6].

The intention of the present investigation was to show that a design procedure based on a BEM model can also provide an adequate description of distributive quantities such as thrust and power distribution. Knowledge about how closely distributions match those obtained by means of CFD analysis is important, for instance, when aerodynamic optimization has to be coupled to numerical or analytical structural optimization. Hence, CFD analysis has been used here as a postanalysis method for assessing BEM results.

II. BEM Design and Analysis Procedures

A. Design Criterion

Betz's [7] assumption of an optimal trailing-vortex system was selected as a design criterion for minimizing induced losses. According to Betz, a propeller having minimal induced losses creates a slipstream of a helical shape of constant wake pitch Λ_1 in a radial direction. However, Λ_1 can change along the axial direction. It is important to note that Λ_1 generally differs from the blade pitch Λ . An interested reader may also consult Wald [8], who has presented a detailed theoretical discussion of the validity of Betz's condition and the dynamics of the shed-vortex system.

Betz's criterion is related to an appropriate blade loading via G_P . G_P is used in the BEM design procedure since it is very quick and simple to obtain for arbitrary values of B and λ and, even more important, shows a reasonable resemblance to G_G at design values of B and λ , as depicted in Fig. 1. A detailed discussion of G_G and G_P is available [8,9].

B. BEM Model

The BEM model is selected as the physical model of propeller action in the following design and analysis procedures. According to the analysis performed by Gur and Rosen [3], a BEM model is selected for its accuracy, simplicity, and numerical efficiency. Although it is by far the simplest of the blade-element (BE) group of models, its results differ only marginally from those provided by other, more complex BE models, like lifting-line or vortex BE models [3]. Numerical efficiency is important, since solving the thus obtained equation system proceeds iteratively. An important advantage of the BEM model is the fact that it can also take into account

Received 11 April 2011; revision received 3 November 2011; accepted for publication 4 November 2011. Copyright © 2011 by the American Institute of Aeronautics and Astronautics, Inc. All rights reserved. Copies of this paper may be made for personal or internal use, on condition that the copier pay the \$10.00 per-copy fee to the Copyright Clearance Center, Inc., 222 Rosewood Drive, Danvers, MA 01923; include the code 0021-8669/12 and \$10.00 in correspondence with the CCC.

*Research Scientist, Faculty of Mechanical Engineering, Laboratory for Aeronautics, Askerceva 6; jurij.sodja@fs.uni-lj.si.

†Research Scientist, Rovsnikova 7; domen.stadler@turboinstitut.si.

‡Assistant Professor, Faculty of Mechanical Engineering, Laboratory for Aeronautics, Askerceva 6; tadej.kosel@fs.uni-lj.si.

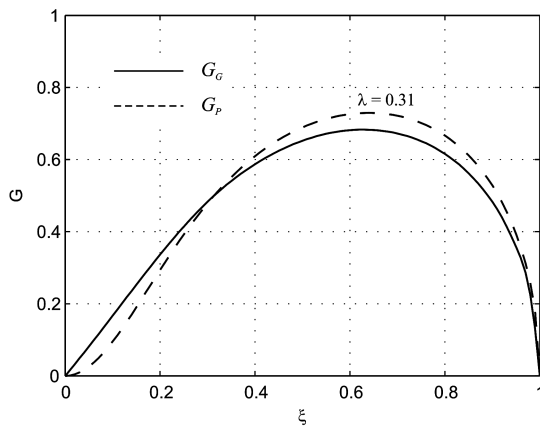


Fig. 1 G_G and G_P at design-point values of $\lambda = 0.31$ and $B = 3$.

hard-to-model aerodynamic effects such as compressibility and viscosity. These effects can be accounted for by using an appropriate airfoil database that contains BE's section aerodynamic properties in terms of M and Re . The BEM model is implemented in the way suggested by Adkins and Liebeck [2]. Detailed explanation of the BEM model in general is offered by Glauert [10].

C. Design and Analysis Procedures

BEM design and analysis procedures are very much alike from a mathematical perspective. They differ only in the quantities that are known and those whose value is searched for. Important quantities are listed in Table 1 where it can be seen clearly how the listed quantities switch roles from parameter to variable in the two complementary procedures. Furthermore, there are more unknowns present in the design procedure. This is expected since the Betz criterion still has to be imposed on the blade design. It should be pointed out that by selecting α so that ϵ is minimized, the viscous losses of the blade are also minimized. α can be selected either in advance or over the course of the design procedure. It is selected in advance if it is decided to neglect the dependence of C_L , C_D , and ϵ on Re and M . Conversely, selecting α during the design procedure allows viscous and compressibility effects to be taken into account in the manner described in Sec. II.B. Unfortunately, this decision is often driven by the fact that an accurate and complete airfoil database for the whole range of Re and M is hard to provide.[§]

BEM analysis enables straight propeller blades of an arbitrary shape to be studied very accurately. One can even model the blade thickness simply by prescribing the appropriate airfoil distribution along the blade.

However, there are also limitations. It was noted that both the BEM design and analysis procedures do not provide any information on the distribution of the chord c around the radial axis of the blade. As a consequence, the shape of the blade is not fully determined by the design procedure, nor it is taken fully into account by the analysis procedure. This drawback is the consequence of the actuator disk concept of the momentum part on which the BEM model is based. This limits the usefulness of the BEM procedure when designing and analyzing swept propeller blades.

III. CFD Analysis

A. Meshing and Discretization Settings

The computational domain given by Fig. 2, was, for the most part, meshed with hexagonal elements. The propeller blade was meshed with prismatic elements in order to ensure quality mesh in the blade's boundary layer. The transition to hexagonal mesh was carried out by tetragonal elements. Important cross sections of mesh used in the CFD simulations are given by Fig. 3.

[§]MH-Aerotools written by Martin Hepperle was used to calculate airfoil characteristics in the analysis procedure. Additional data available at <http://www.mh-aerotools.de/airfoils/> [retrieved Jan. 2011].

Table 1 Design and analysis parameters and variables

Parameter	Design	Analysis
<i>Geometry parameters</i>		
c	? ^a	✓ ^b
Airfoil	✓	✓
R	✓	✓
R_H	✓	✓
β	?	✓
B	✓	✓
<i>Airfoil parameters</i>		
Thickness	✓	✓
α	?/✓	?
C_L	✓	?
C_D	✓	?
ϵ	✓	?
<i>Performance parameters</i>		
n	✓	✓
v_0	✓	✓
C_T	✓/?	?
C_P	?/✓	?
η	?	?

^a? implies that the parameter is searched for.

^b✓ implies that the parameter is prescribed.

Advection terms were calculated using a high-resolution advection scheme: a blend of first- and second-order upwind Euler advection schemes. Turbulence equations were treated with a first-order upwind discretization scheme. Transient terms were discretized using a second-order backward Euler scheme with automatic time-step initialization. If the Courant number evaluated to a value of less than 5, a time step was initialized with values of a previous time step. Otherwise the time step was initialized by means of extrapolation based on previous time steps.

B. CFD Analysis Settings

CFD analyses were set up using ANSYS CFX. Settings were chosen according to best-practice recommendations [11]. Analyses were performed in two steps. First, stationary CFD analyses were carried out. These were used as initial conditions in transient analyses, in which a stationary solution was propagated in time for another 20 revolutions of the propeller. Because of the extremely lengthy nature of transient calculations, the time step was selected near the upper limit of $1/\Omega$, which evaluated to 2.5×10^{-4} s. Therewith the time resolution of the developed flow was obtained. Convergence criteria were set to 1×10^{-5} s and 1×10^{-4} rms in stationary and transient analyses, respectively.

Turbulence was accounted for by a $k-\epsilon$ turbulence model. The type of averaging in this model depended on the type of analysis performed. Time-averaging was applied in the stationary analyses, whereas ensemble averaging was applied in the transient analyses, which greatly reduced the damping of vortical structures in the flow. The effect of damping is presented later.

The boundary layer was treated by scalable wall functions. These were reported to efficiently solve the y^+ value problem in the boundary mesh elements [11]. Near-wall mesh elements could thus be of arbitrary thickness, which simplified the meshing process greatly.

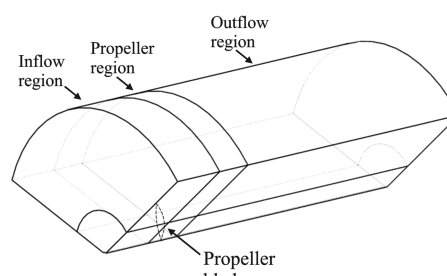


Fig. 2 Computational domain.

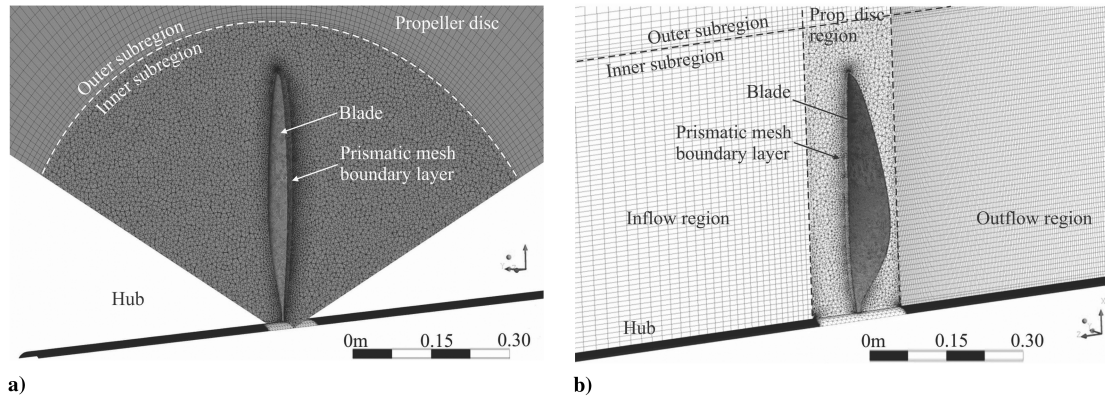


Fig. 3 Mesh used in CFD simulations.

A rotating propeller was simulated by placing the whole computational domain in a rotating frame of reference having an appropriate value of Ω . According to the ANSYS recommendations [11], an alternate rotation model was used in order to improve convergence.

IV. Results

A. Validation

BEM and CFD predictions were validated by comparison with experimental results. To ensure comparability with Adkins and Liebeck's [2] results, the same set of experimental results prepared by Reid [12] was chosen. Figures 4–6 display the dependence of C_T , C_P , and η on J . Evidently, CFD results match the experiment much more closely than the BEM results in all cases. Nevertheless, the BEM results also follow the experiment very well in terms of trend. The propeller used NACA 16-series airfoils with design $C_L = 0.7$. Only a limited range of aerodynamic characteristics was found for this family of airfoils [13]. Hence, the BEM model is only validated over a limited range of advance ratios.

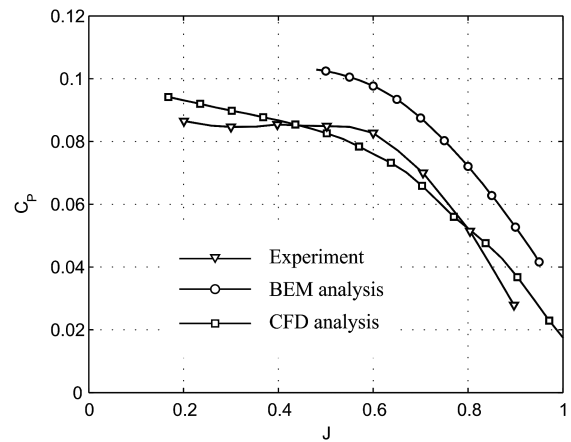
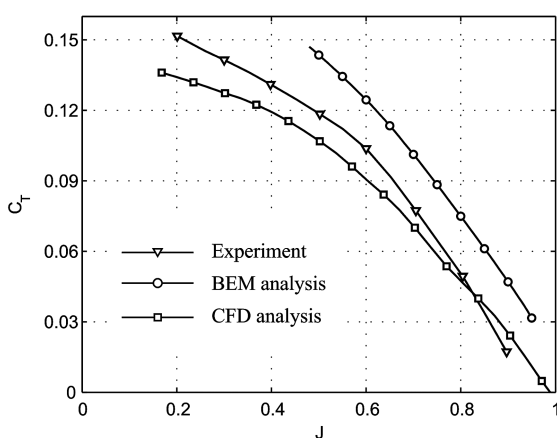
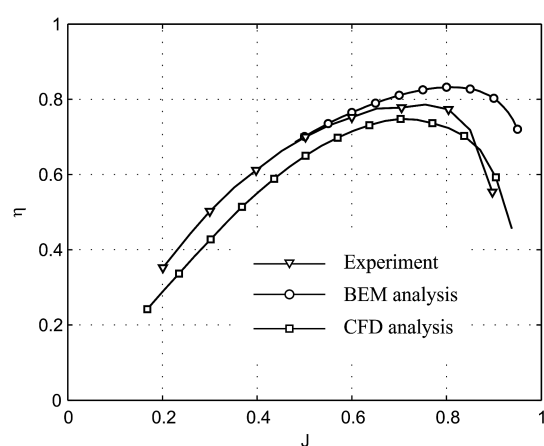
Figures 7 and 8 display the validation for $\partial C_T / \partial \xi$ and $\partial C_P / \partial \xi$. Surprisingly, the BEM analysis matches the experiment more closely than CFD for both $\partial C_T / \partial \xi$ and $\partial C_P / \partial \xi$ and for both $J = 0.6$ and 0.8 . It would be expected that the CFD analysis would fit the experiment better, since a better match between CFD and experiment was demonstrated in the case of integral results. The difference may be attributed to the fact that C_T and C_P were measured directly by means of force and torque balances, whereas $\partial C_T / \partial \xi$ and $\partial C_P / \partial \xi$ were determined indirectly by measuring the flowfield behind the propeller using an array of pitot tubes [12].

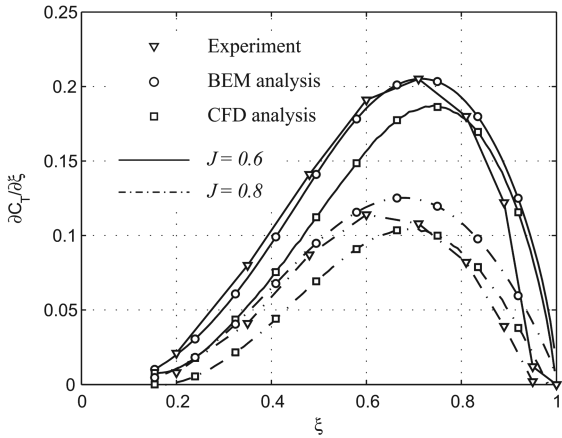
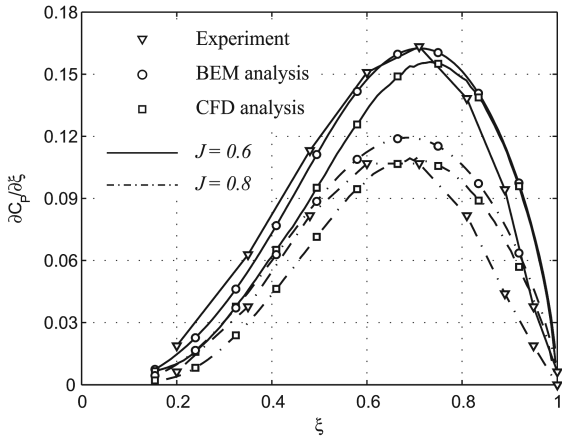
B. Design Optimality

The design point was selected with the intention of having values typical for ultralight aviation. Design parameters and working

conditions with which the propeller had to comply are defined in Table 2.

Design optimality was assessed by investigating w , λ_1 , Γ , and G . w , and λ_1 were chosen since they reflect specific wake properties. If the propeller is designed according to Betz's condition, w and λ_1 are presumed to be constant, along ξ_1 . w , and λ_1 are derived independently out of induced velocities by considering Fig. 9 and following Eqs. (1) and (2) [8]. They therefore reflect the consistency in behavior of the Betz criterion, the BEM model, and the CFD analyses. Γ and G were chosen since they reflect the loading conditions along the blade. By rewriting and recalculating Γ in the form of G , one achieves a direct comparison between the actual G and G_G . Γ and G are calculated separately out of the thrust and power

Fig. 5 Validation of dependence of C_p on J .Fig. 4 Validation of dependence of C_t on J .Fig. 6 Validation of dependence of η on J .

Fig. 7 Validation of dependence of $\partial C_T / \partial \xi$ on ξ .Fig. 8 Validation of dependence of $\partial C_P / \partial \xi$ on ξ .

distribution, $dT/d\xi$ and $dP/d\xi$, by following Eqs. (3) and (4), as given by Wald [8]:

$$w^2 \cos^2 \phi = u_a^2 + u_\phi^2 \quad (1)$$

$$\tan \phi = \lambda_1 / \xi \quad (2)$$

$$B\Gamma = \frac{1}{\rho} \frac{1}{\Omega r - u_\phi} \frac{dT}{R d\xi} = \frac{1}{\rho} \frac{1}{v_0 + u_0} \frac{1}{R \xi} \frac{dQ}{R d\xi} \quad (3)$$

Table 2 Optimization design points

Parameter	Value
<i>Propeller parameters</i>	
D	1 m
B	3
Airfoil	Clark Y
<i>Airfoil parameters^a</i>	
α	3°
C_L	0.548
C_D	0.0257
ϵ	21.3
<i>Working conditions</i>	
v_0	40 m/s
n	2400 rpm
J	1
P	10 kW
C_P	0.132

^aAirfoil characteristics were obtained from MH-Aerotools written by Martin Hepperle. Additional data available at <http://www.mh-aerotools.de/airfoils/> [retrieved January 2011].

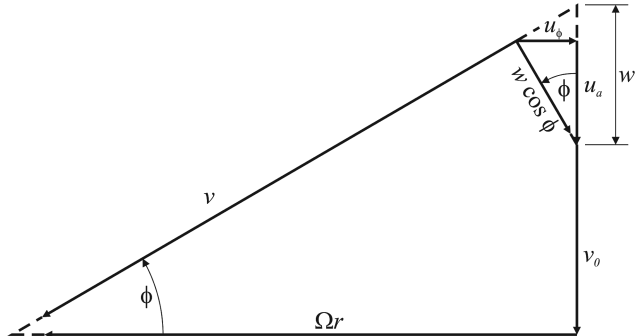


Fig. 9 Velocity components at the helicoidal vortex sheet [8].

$$G = \frac{B\Gamma\Omega}{2\pi w(v_0 + w)} \quad (4)$$

The results are presented in Fig. 10.

BEM values of w and λ_1 follow predictions very well, which is logical, since the design process relies on enforcing the correct geometry of the trailing-vortex sheets. On the other hand, the CFD results of w and λ_1 exhibit a significant variation along the blade. Observing Fig. 10a it appears, for regions close to the root and tip of the blade, as if the vortex wake is propagated backward into the propeller disk instead away from it. There is also an evident variation in w along the blade radius. The CFD prediction of λ_1 exhibits more constant behavior: at least for the interval of ξ between 0.3 and 0.95. This is interesting, since λ_1 is linearly dependent on w , see Eq. (5), as given by Wald [8]:

$$\lambda_1 = \frac{v_0 + w}{\Omega R_1} \quad (5)$$

Similar behavior of BEM and CFD results is observed in the case of Γ . BEM results overestimate CFD results over the entire blade. It is interesting to note that theoretical results yield different values of Γ , depending on whether Γ is calculated from $dT/d\xi$ or $dP/d\xi$, which is considered to be a discrepancy in the BEM model. Similar behavior of the BEM is also observed in the case of G . CFD results for both Γ and G are consistent in this respect.

Comparison of BEM results in Fig. 10d with those in Fig. 1 identifies the effect of using G_P instead of G_G . Conversely, G obtained via CFD analyses does not resemble G_G or G_P very well in any case. The reason is believed to lie in the dependence of the circulation function on the field of induced velocities. An emanating vortex system should form a helicoidal surface having constant Λ_1 . Such a vortex system may be considered only as an idealized transient state. Therefore, it rolls up into the tip and axial vortices. However, the roll-up effect of the trailing-vortex sheets should not influence the induced flowfield near the propeller disk plane if the roll-up occurs far enough from the propeller and if the hydrodynamic impulse is conserved [8]. On the other hand, CFD visualizations of the propeller slipstream in Fig. 11 suggest that the roll-up takes place far too quickly in reality. Therefore, the induced velocities (and hence w , λ_1 , and G) are all influenced by this effect.

C. Integral Results

The dependences of C_T , C_P , and η on J were determined (Figs. 12–14). It is evident that the CFD results for C_T , C_P , and η match the predictions of the BEM model very well around the specified design point (Table 2). It is evident that for $J < 1$, CFD analysis predicts lower values of C_T than the BEM analysis. However, both C_T and C_P , as determined by CFD analysis, are overpredicted relative to the BEM analysis for $J > 1$. C_T , C_P , and η , as calculated by CFD, all depart significantly from theoretical predictions for $J \gg 1$. Furthermore, three distinct working modes of the propeller are identified by both BEM and CFD analyses. In the range where $J_{BEM} < 1.35$ and $J_{CFD} < 1.5$, the propeller operates in a

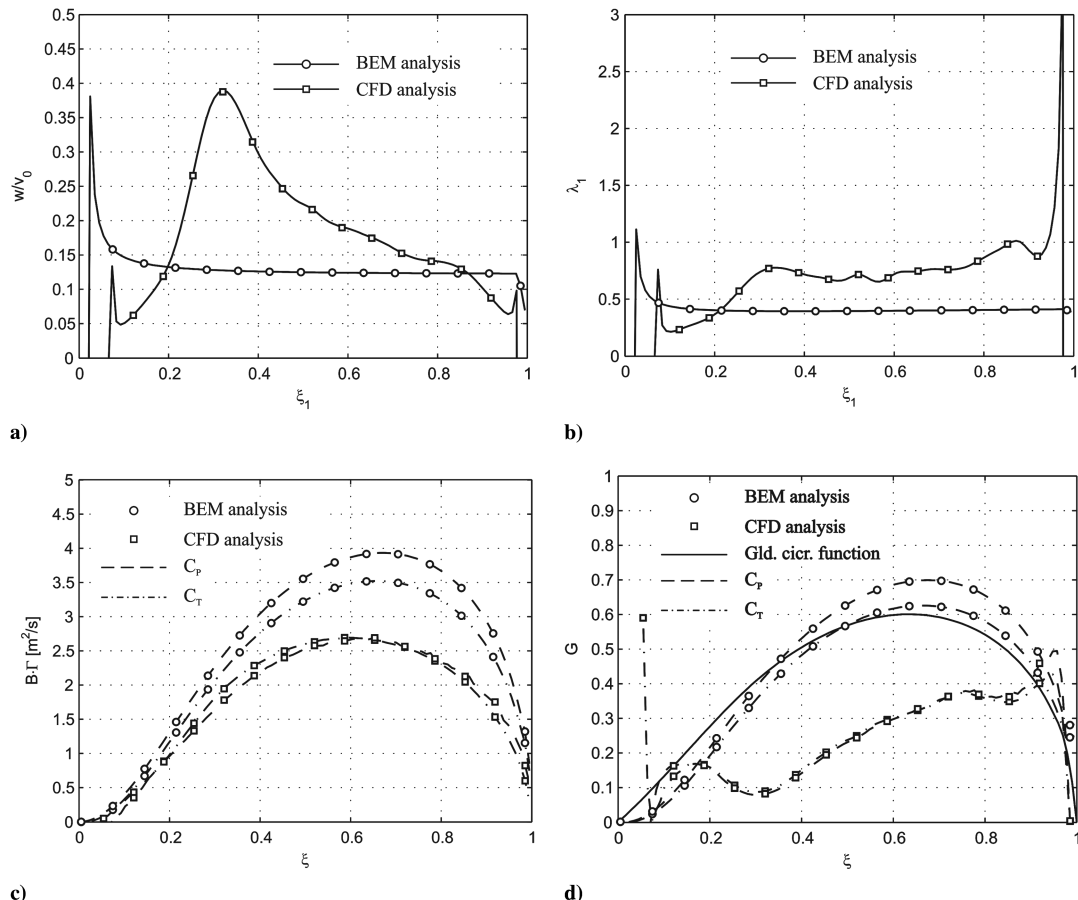


Fig. 10 a) Wake axial displacement velocity, b) wake advance ratio, c) circulation distribution, and d) circulation function.

propeller mode producing useful thrust. For $1.35 < J_{BEM} < 1.41$ and $1.5 < J_{CFD} < 1.57$, the propeller operates in a brake mode. Thrust opposing forward movement is produced. However, there is still power required to keep the propeller turning. For $J_{BEM} > 1.41$ and $J_{CFD} > 1.57$, the propeller operates in windmill mode. Negative thrust is produced by the propeller, but turning power can be extracted from the flow passing through the propeller disc. Individual operating modes are marked in Fig. 14. The brake mode is specifically marked by a gray stripe separating the propeller and windmill mode. It is important to point out that propeller and windmill efficiencies are defined differently. Propeller efficiency is defined by Eq. (6) as the ratio of useful power produced by the propeller to the power needed to keep the propeller turning. However, windmill efficiency is defined by Eq. (7) as the ratio of useful power

extracted from the airflow by the rotor to the total amount of power available in the airflow passing through the rotor disk [14]:

$$\eta_{\text{propeller}} = JC_T / C_P \quad (6)$$

$$\eta_{\text{windmill}} = \frac{P}{\frac{1}{2} \rho v_0^3 S} \quad (7)$$

D. Distributive Results

Loading conditions along the propeller blade at different values of J are presented in Figs. 15 and 16. Even though there is fairly good agreement between BEM and CFD analyses regarding integral quantities, there are some significant differences among their

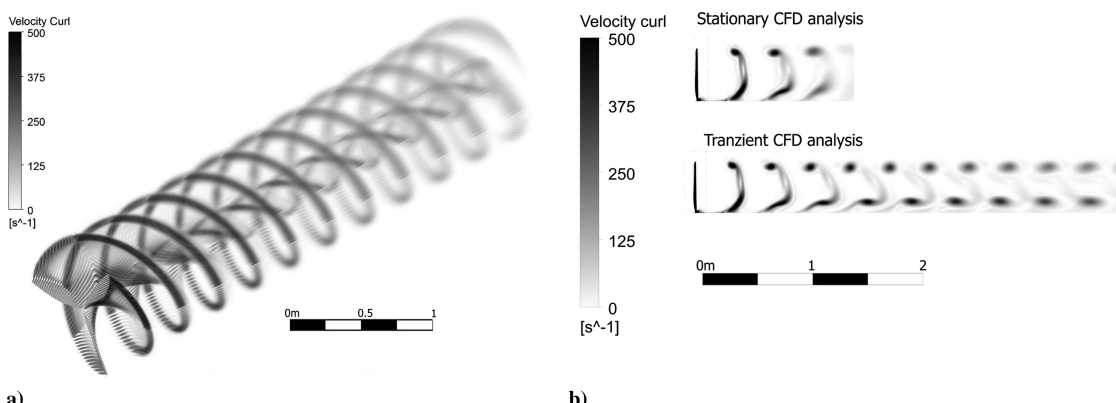
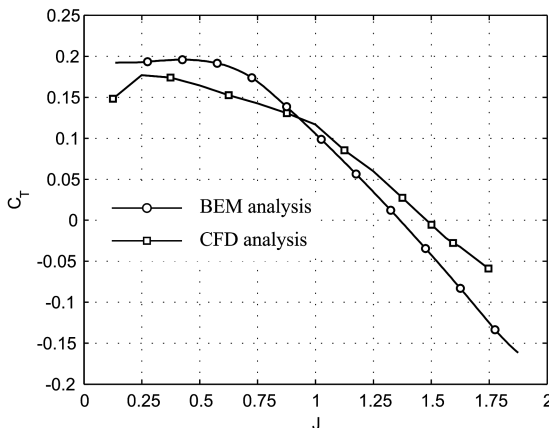
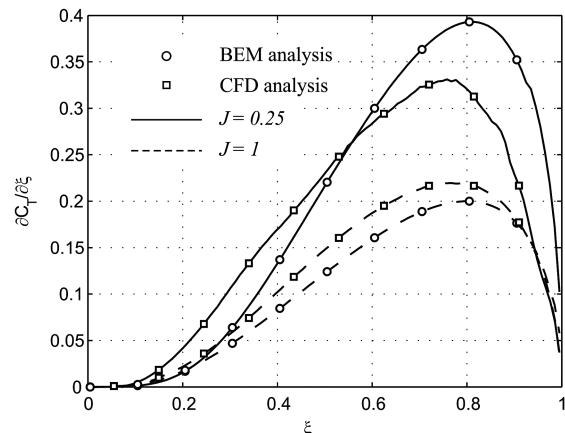
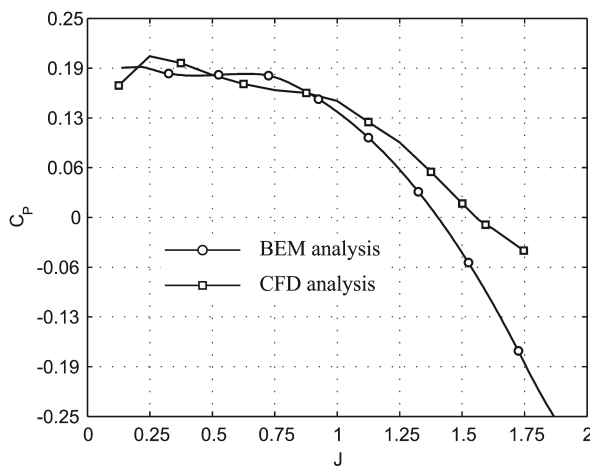
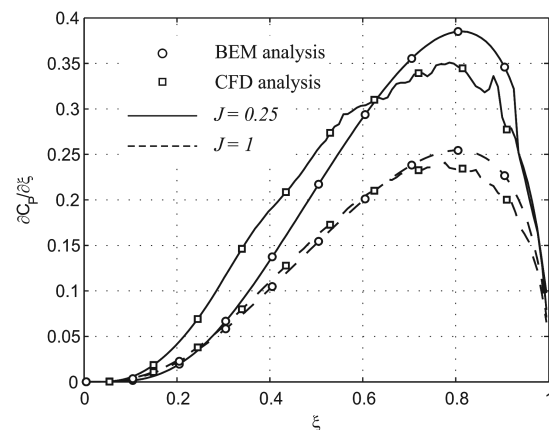
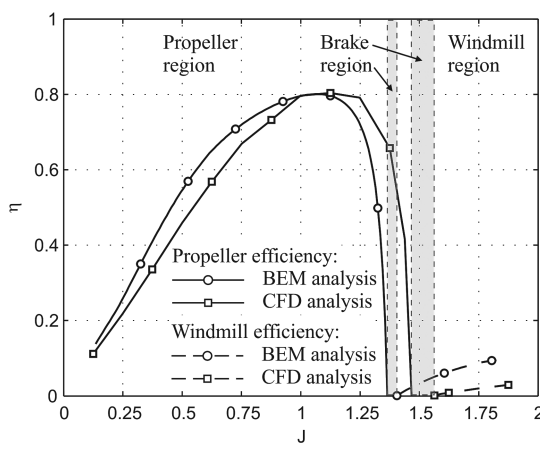


Fig. 11 a) Vortex sheets emanating from propeller blades and b) the effect of damping on emanated vortex sheets due to Reynolds-averaged Navier-Stokes averaging.

Fig. 12 Dependence of C_T on J .Fig. 15 Dependence of $\partial C_T / \partial \xi$ on ξ .Fig. 13 Dependence of C_P on J .Fig. 16 Dependence of $\partial C_P / \partial \xi$ on ξ .

respective distributions along the propeller blade in both quantitative and qualitative senses.

Qualitatively, CFD results indicate that loads due to C_T and C_P are more evenly distributed over a larger portion of the blade, whereas theoretical predictions indicate that the bulk of the load is concentrated in the outer part of the blade. Furthermore, peak values of $\partial C_T / \partial \xi$ and $\partial C_P / \partial \xi$ tend to shift slightly to the middle of the blade according to CFD analysis. However, both load redistribution and peak shift are more pronounced at lower values of J and become almost negligible as the value of J is increased.

Fig. 14 Dependence of η on J .

V. Conclusions

Over the course of validation, the CFD method provides better results than the BEM, as far as integral C_T , C_P , and η are concerned. On the other hand, BEM yields a better match with experiment, as far as distributive $\partial C_T / \partial \xi$ and $\partial C_P / \partial \xi$ are concerned. This is surprising. One possible reason is identified in the two different methods used to obtain the two groups of experimental results. As far as validation is concerned, it is important to report that we could not obtain the same quality of BEM results as was reported in the referenced literature, although the geometry of the experimental propeller was replicated carefully and experimental characteristics of the adequate NACA 16-series airfoils were used.

In the case of BEM design procedure, CFD analysis results yield remarkably sufficient agreement between both integral and distributive quantities. However, inspection of the physical assumptions arising from the Betz optimization criterion reveals a significant departure of CFD results from BEM predictions and the Betz condition. Neither w nor λ_1 are constant along the blade radius, nor does the circulation function resemble G_G or G_P in the case of CFD results. The difference is believed to be the consequence of the more realistic treatment of vortex structures in the very close vicinity of the propeller in the case of CFD analysis. It is there that the shed vorticity and its topology have the strongest influence on the flowfield around the blades. It remains to investigate whether CFD analyses are able to deliver further improvement in terms of efficiency, thrust, and power of the propeller if the geometry of the blades were changed in such a way that CFD distributive results would be consistent with the Betz optimization criterion.

Comparison between CFD analysis and BEM analysis reveals that both integral and distributive results are fairly consistent over a wide range of working conditions. Hence, the comparison also reveals the potential of the BEM model in fluid-structure interaction predictions.

We believe that the BEM model could be successfully coupled with some sort of structural solver in order to form a rapid-design and analysis tool for propellers and other rotary-wing devices.

References

- [1] Larrabee, E. E., "Five Years Experience with Minimum Induced Loss Propellers—Part I: Theory," Society of Automotive Engineers, TP 840026, 1984.
- [2] Adkins, C. N., and Liebeck, R. H., "Design of Optimum Propellers," *Journal of Propulsion and Power*, Sept.–Oct. 1994, pp. 676–682; also AIAA Paper 1983-0190, Jan. 1983.
doi:10.2514/3.23779
- [3] Gur, O., and Rosen, A., "Comparison Between Blade-Element Models of Propellers," *The Aeronautical Journal*, Vol. 112, No. 1138, Dec. 2008, pp. 689–704.
- [4] Westmoreland, W. S., Tramel, R. W., and Barber, J., "Modeling Propeller Flow-Fields Using CFD," AIAA Paper 2008-402, Jan. 2008.
- [5] Sezer-Uzol, N., and Long, L. N., "3-D Time-Accurate CFD Simulations of Wind Turbine Rotor Flow Fields," AIAA Paper 2006-394, Jan. 2006.
- [6] Roosenboom, E. W. M., Stürmer, A., and Schröder, A., "Advanced Experimental and Numerical Validation and Analysis of Propeller Slipstream Flows," *Journal of Aircraft*, Vol. 47, No. 1, Jan.–Feb. 2010, pp. 284–291; also AIAA Paper 2009-3626, June 2009.
doi:10.2514/1.45961
- [7] Betz, A., "Screw Propellers with Minimum Energy Loss," *Goettingen Reports*, 1919, pp. 193–213.
- [8] Wald, Q. R., "The Aerodynamics of Propellers," *Progress in Aerospace Sciences*, Vol. 42, 2006, pp. 85–128.
doi:10.1016/j.paerosci.2006.04.001
- [9] Johnson, W., "Vortex Theory," *Helicopter Theory*, Dover, New York, 1994, pp. 72–91.
- [10] Glauert, H., "Airplane Propellers," *Aerodynamic Theory*, Div. L, Vol. 4, Dover, New York, 1963, pp. 169–269.
- [11] *ANSYS CFX Reference Guide*, ANSYS, Inc., Canonsburg, PA, 2009.
- [12] Reid, E. G., "The Influence of Blade-Width Distribution on Propeller Characteristics," NACA TN 1834, March 1949.
- [13] Lindsey, W. F., Stevenson, D. B., and Daley, B. N., "Aerodynamic Characteristics of 24 NACA 16-Series Airfoils at Mach Numbers Between 0.3 and 0.8," NACA TN 1546, Sept. 1948.
- [14] Hansen, M. O. L., "1-D Momentum Theory for an Ideal Wind Turbine," *Aerodynamics of Wind Turbines*, 2nd ed., Earthscan, London, 2008, pp. 27–40.